Graefes Arch Clin Exp Ophthalmol (2016) 254:1941–1949
DOI 10.1007/s00417-016-3343-9

RETINAL DISORDERS

# Prevalence, characteristics, and pathogenesis of paravascular inner retinal defects associated with epiretinal membranes

**Yukiko Miyoshi[1] · Akitaka Tsujikawa[1] · Saki Manabe[1] · Yuki Nakano[1] · Tomoyoshi Fujita[1] · Chieko Shiragami[1] · Kazuyuki Hirooka[1] · Akihito Uji[2] · Yuki Muraoka[2]**

Received: 10 February 2016 / Revised: 27 March 2016 / Accepted: 4 April 2016 / Published online: 19 April 2016


**Abstract**
*Purpose* To investigate the prevalence, detailed characteristics, and pathogenesis of paravascular inner retinal defects (PIRDs) in eyes with epiretinal membranes (ERMs).
*Methods* In this prospective observational case series, we included 81 eyes of 81 patients with idiopathic ERMs, without high myopia. The retinal structure surrounding the PIRDs was assessed using sequential thin sectioning of optical coherence tomography. The PIRDs were classified into three grades. Typical defects of the inner retinal tissue were defined as grade 3. Inner retinal cleavages with openings to the vitreous cavity and no apparent defect of the inner retinal tissue were defined as grade 2. Inner retinal cleavages or cystoid spaces with no connection to the vitreous cavity were defined as grade 1.
*Results* Of 81 eyes with ERMs, 31 (38.3 %) had PIRDs along the temporal arcade vessels (grade 1 in six eyes, grade 2 in four eyes, and grade 3 in 21 eyes). PIRDs were frequently accompanied by broad defects of the inner retinal tissue (grade 3). Although some ERMs directly adhered to the edge of a PIRD or the retinal vessels, PIRDs were often located outside the area of adhesion to the ERM. In some OCT sections, vitreous traction on the inner retina seemed to contribute to the progression of PIRDs. Visual field abnormalities corresponded to the location of the PIRDs in 44.4 % of eyes with grade 3 PIRDs.
*Conclusions* Deviation of retinal vessels due to the traction of the ERMs may contribute to the pathogenesis of PIRDs. PIRDs often cause visual field abnormalities corresponding to the location of the defect.

**Keywords** Epiretinal membrane · Optical coherence tomography · Paravascular inner retinal defect

## Introduction

Using sequential thin sectioning with optical coherence tomography (OCT), Muraoka et al. [1] recently reported the characteristics and pathogenesis of inner retinal defects along the major retinal vessels in eyes with high myopia. The authors designated these lesions as paravascular inner retinal defects (PIRDs). In eyes with high myopia, deviation of retinal vessels due to axial elongation contributes to the pathogenesis of PIRDs. PIRDs may partially overlap with retinal lesions previously described as cleavage of the retinal nerve fiber layer [2, 3], inner retinal cleavage [4–6], pseudodefects of the retinal nerve fiber layer [7], paravascular retinal cysts [8], or lamellar holes [9]. Because PIRDs are not simple cleavages of the inner retinal tissue, and are often accompanied by a functional abnormality, the term PIRD more precisely describes the characteristic features of the lesions [1].

In the same study, the authors also reported 15 cases of PIRDs associated with epiretinal membranes (ERMs) in eyes without high myopia [1]. The tractional force induced by an ERM may cause deviation of the retinal vessels toward the central macula, leading to the formation of PIRDs adjacent to the temporal arcade vessels. In addition, Komeima et al. [4] reported a case of paravascular inner retinal cleavage associated

✉ Akitaka Tsujikawa
tujikawa.kagawa@gmail.com

[1] Department of Ophthalmology, Kagawa University Faculty of Medicine, 1750-1 Ikenobe, Miki-cho, Kagawa, Japan

[2] Department of Ophthalmology and Visual Sciences, Kyoto University Graduate School of Medicine, Kyoto, Japan

with an ERM, and Hwang et al. [6] also reported six cases of inner retinal cleavage in eyes with ERMs. However, all of these reports are case series, and limited information is available on the prevalence, detailed characteristics, and pathogenesis of PIRDs associated with ERMs. In the current study, we prospectively investigated consecutive eyes with idiopathic ERMs without high myopia using sequential OCT sectioning, and studied the effect of PIRDs on visual function.

## Patients and methods

### Patients

This prospective study comprised 81 consecutive patients (81 eyes) with idiopathic ERMs who were examined at the Department of Ophthalmology of Kagawa University Hospital between January 2015 and July 2015. Based on the original report on PIRDs [1] and other reports on similar lesions [3–9], we expanded the definition of PIRD in the current study. Typically, a PIRD was defined as a defect of the inner retina adjacent to the major retinal vessels that was disconnected from the optic disc and seen in eyes with high myopia or ERMs. We also included inner retinal cleavages or cystoid spaces within the inner retina along the major retinal vessels, which were detected on OCT examination, and we considered these lesions to represent different grades of PIRDs.

The current study included only eyes with idiopathic ERMs. Eyes with secondary ERMs (i.e., secondary to diabetic retinopathy, retinal vein occlusion, uveitis, rhegmatogenous retinal detachment, retinal break, history of retinal laser photocoagulation and cryopexy, or Coats' disease) were excluded. Eyes with high myopia (refractive error of less than −6 diopters or an axial length of more than 26.5 mm), eyes with glaucoma, and eyes with a history of ocular surgery other than cataract surgery were also excluded from the current study.

Each patient underwent a comprehensive ophthalmic examination to obtain measurements of best-corrected visual acuity (VA) using a Landolt chart, refractive error, keratometry, axial length using partial coherence interferometry (IOLMaster; Carl Zeiss Meditec, Jena, Germany), and intraocular pressure using a Goldmann applanation tonometer. Fundus biomicroscopy with a non-contact lens, 45° digital fundus photography (TRC-50LX; Topcon, Tokyo, Japan), and detailed OCT examinations (Spectralis HRA+OCT; Heidelberg Engineering, Heidelberg, Germany) were performed after pupil dilation. In eyes with PIRDs, a visual field test using Goldmann perimetry was also performed.

### OCT examination of PIRDs

In each eye with an ERM, the posterior pole was first examined using Spectralis HRA+OCT with a novel extended field imaging (EFI) OCT technique [10]. Briefly, this technique involves imaging the posterior pole through trial frames fitted with a +20-diopter lens. The placement of a convex lens between the eye and the OCT probe increases the imaging light incidence angle, resulting in expansion of the imaging field. With the use of Spectralis HRA+OCT, the EFI technique allowed us to capture images with a 1.45-fold to 1.49-fold increased scan length compared to conventionally obtained images [10].

To comprehensively detect the PIRDs, the posterior pole and paravascular areas of both the superotemporal and inferotemporal arcade vessels were examined with dense radial scanning by Spectralis HRA+OCT using the EFI technique (Fig. 1). When PIRDs were detected using the EFI technique, the retinal structure surrounding the PIRDs was assessed in detail using Spectralis HRA+OCT without the

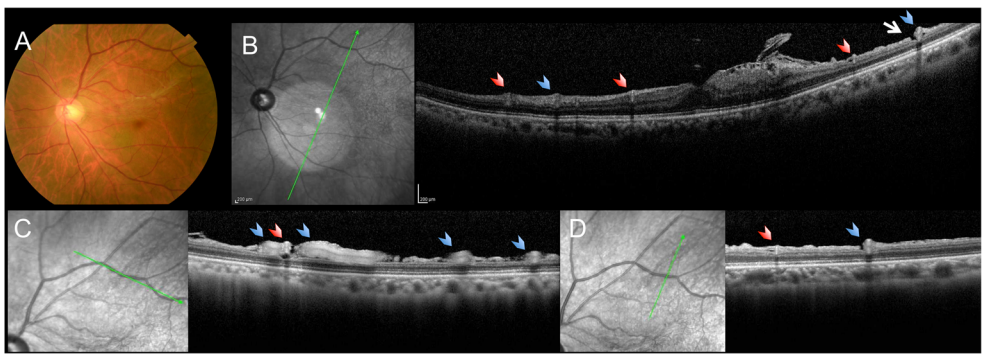


**Fig. 1** Examination of paravascular inner retinal defects (PIRDs) associated with epiretinal membranes (ERMs) using optical coherence tomography (OCT). **a** An eye with an idiopathic ERM. **b** In each eye with an ERM, the posterior pole was first examined using the novel extended field imaging (EFI) OCT technique. The EFI technique allowed us to capture the images with 1.45-fold to 1.49-fold greater scan length than that of conventional OCT images. **c**, **d** When PIRDs were detected, the retinal structure surrounding the PIRDs was assessed in detail using OCT without the EFI technique at longitudinal sections parallel to and cross sections vertical to the major retinal vessels. *White arrow* = PIRD, *red arrowhead* = retinal artery, *blue arrowhead* = retinal vein

EFI technique on the sections that were longitudinal and traverse to the major retinal vessels. The B-scans of the PIRDs were sequentially and thinly imaged (minimum 49 sections measuring 5°), and the mean image generated from at least 20 B-scans of a single area was then analyzed [11–13].

The presence or absence of posterior vitreous detachment (PVD) or vitreoretinal adhesion was determined based on these sequential OCT sections and peripapillary circular OCT sections. We confirmed the presence of PVD when the posterior vitreous membrane was completely detached at the optic disc, even if some vitreous adhesions were persistent around the PIRDs.

The PIRDs were classified into three grades based on the OCT examinations. On OCT, defects of the inner retinal tissue adjacent to the major retinal vessels were defined as grade 3 PIRDs (Fig. 2). Inner retinal cleavages along the major retinal vessels with openings to the vitreous cavity, with no apparent defect of the inner retinal tissue were defined as grade 2 PIRDs. Inner retinal cleavages or cystoid spaces along the major retinal vessels that showed no connection to the vitreous cavity were defined as grade 1 PIRDs. In eyes with multiple PIRDs, the higher grade was used as the grade of the eye.

### Statistics

All values are presented as the means ± standard deviation. The statistical analysis was performed using IBM SPSS Statistics 21 (IBM Corp., Armonk, NY, USA). For statistical analysis, the VA measured with a Landolt chart was converted to a logarithm of the minimum angle of resolution (logMAR). The Student *t* test was performed to compare quantitative data that were normally distributed and had equal variance. Significant differences in the sampling distributions were determined using the chi-square test. A $p$ value of less than 0.05 was considered to be statistically significant.

## Results

In the current study, we evaluated 81 eyes of 81 subjects with idiopathic ERMs (44 women and 37 men) aged 52–86 (71.6 ± 8.4) years (Table 1). Eyes with high myopia were not included, and the mean axial length was 23.48 ± 0.91 mm. Nine eyes were pseudophakic.

Of 81 eyes with ERMs, 31 (38.3 %) had PIRDs along the temporal arcade vessels. No PIRDs were seen in more nasal retina than the optic disc. PIRDs along the temporal arcade vessels were more frequently detected in the superior hemisphere than in the inferior hemisphere; 13 eyes had PIRDs only in the superior hemisphere, 5 eyes had PIRDs only in the inferior hemisphere, and the remaining 13 eyes had PIRDs in both hemispheres. In photographs of the fundus, most

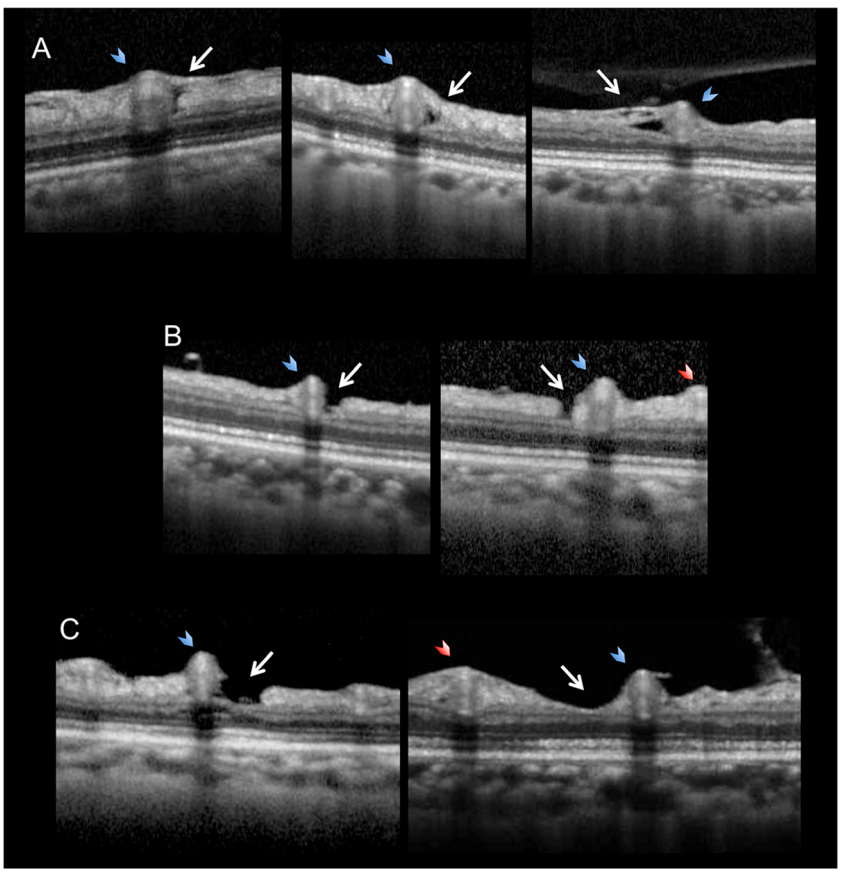


**Fig. 2** Grading of paravascular inner retinal defects (PIRDs) associated with epiretinal membranes (ERMs) using optical coherence tomography (OCT). **a** Inner retinal cleavages or cystoid spaces within the inner retina along the major retinal vessels that showed no connection to the vitreous cavity were defined as grade 1 PIRDs. **b** Inner retinal cleavages along the major retinal vessels with openings to the vitreous cavity, with no apparent defect of the inner retinal tissue, were defined as grade 2 PIRDs. **c** Defects of the inner retinal tissue adjacent to the major retinal vessels were defined as grade 3 PIRDs. In eyes with multiple PIRDs, the highest grade was used as the grade of the eye. *White arrow* = PIRD, *red arrowhead* = retinal artery, *blue arrowhead* = retinal vein

**Table 1** Ocular and general examination findings of patients with epiretinal membranes included in the study

| | Total | PIRD (+) | PIRD (−) |
|---|---|---|---|
| Number of eyes | 81 | 31 | 50 |
| Age, years | 71.6 ± 8.4 | 70.2 ± 8.6 | 72.5 ± 8.2 |
| Gender, women/men | 44/37 | 16/15 | 28/22 |
| Systemic hypertension, *n* (%) | 34 (42.0 %) | 12 (38.7 %) | 22 (44.0 %) |
| Diabetes mellitus, *n* (%) | 11 (13.6 %) | 5 (16.1 %) | 6 (12.0 %) |
| Hyperlipidemia, *n* (%) | 9 (11.1 %) | 3 (9.7 %) | 6 (12.0 %) |
| Visual acuity, logMAR | 0.24 ± 0.20 | 0.28 ± 0.24 | 0.22 ± 0.17 |
| Central retinal thickness, μm | 424.5 ± 85.6 | 463.0 ± 97.1* | 400.6 ± 68.3 |
| Axial length, mm | 23.48 ± 0.91 | 23.47 ± 0.89 | 23.48 ± 0.94 |
| Posterior vitreous detachment, *n* (%) | 64 (79.0 %) | 22 (71.0 %) | 42 (84.0 %) |
| Pseudophakia, *n* (%) | 9 (11.1 %) | 3 (9.7 %) | 6 (12.0 %) |

*PIRD* paravascular inner retinal defect, *logMAR* logarithm of the minimum angle of resolution

*$p < 0.01$, compared with PIRD (−) group

PIRDs appeared as spindle-shaped dark areas along the major retinal vessels and were disconnected from the optic disc. PIRDs were seen along both temporal arcade veins and arteries, but they were more frequently seen along the arcade veins. Eyes with PIRDs had greater central retinal thickness than eyes without PIRDs ($p = 0.003$). Additionally, the VA was somewhat lower in eyes with PIRDs, but the difference was not statistically significant ($p = 0.23$).

On traverse OCT sections of the retinal arcade vessels, PIRDs typically appeared as cystoid or fissure-like spaces with or without an inner retinal surface. However, longitudinal OCT sections along major retinal vessels sometimes revealed that PIRDs were accompanied by broad

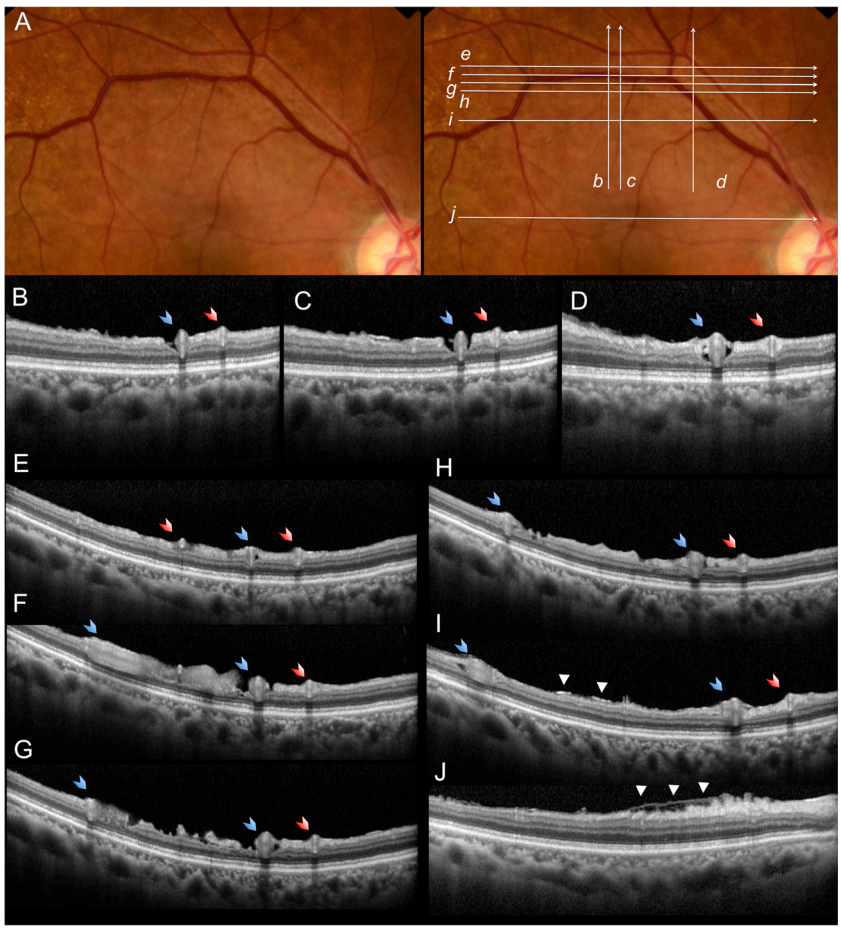


**Fig. 3** A grade 3 paravascular inner retinal defect (PIRD) associated with an epiretinal membrane (ERM). **a** Fundus imaging shows the PIRD along the superotemporal vein (VA, 0.5 on the Landolt chart; axial length, 22.00 mm). Optical coherence tomography (OCT) sections were taken along the *white arrows* (*b*–*j*). **b**–**d** Cross-sectional OCT images show a defect of the inner retina along both sides of the superotemporal vein. **e**–**j** Longitudinal OCT sections show a broad defect of the inner retinal tissue. The PIRD was detected outside the area that adhered to the ERM (*white arrowheads*). The OCT sections show neither direct adhesion of the ERM to the edge of the PIRD nor posterior vitreous adhesion to the PIRD. *White arrow* = PIRD, *red arrowhead* = retinal artery, *blue arrowhead* = retinal vein

defects of the inner retinal tissue (these eyes were categorized as grade 3). In addition, some PIRDs were accompanied by cleavages in the outer plexiform layer. In all of our patients, while ERMs existed at the macular area, PIRDs were often located outside the area that adhered to the ERMs (Fig. 3). In such eyes, OCT rarely showed that the ERM directly adhered to the edge of the PIRD or the retinal vessels; instead, the ERM seemed to exert traction toward the fovea on the inner retina, resulting in the formation of inner retinal cleavages or cystoid spaces. However, upon detailed examination by OCT, several PIRDs appeared to exist at paravascular areas unrelated to the traction vector induced by the ERM.

OCT examinations revealed the role of vitreous traction on the inner retina in the progression of PIRDs (Fig. 4). Of six eyes with grade 1 PIRDs, three (50.0 %) showed vitreous adhesion to major retinal vessels accompanied by PIRDs. In some eyes, the inner surface of PIRDs appeared to be close to being torn off by the vitreous traction. In contrast, no vitreous

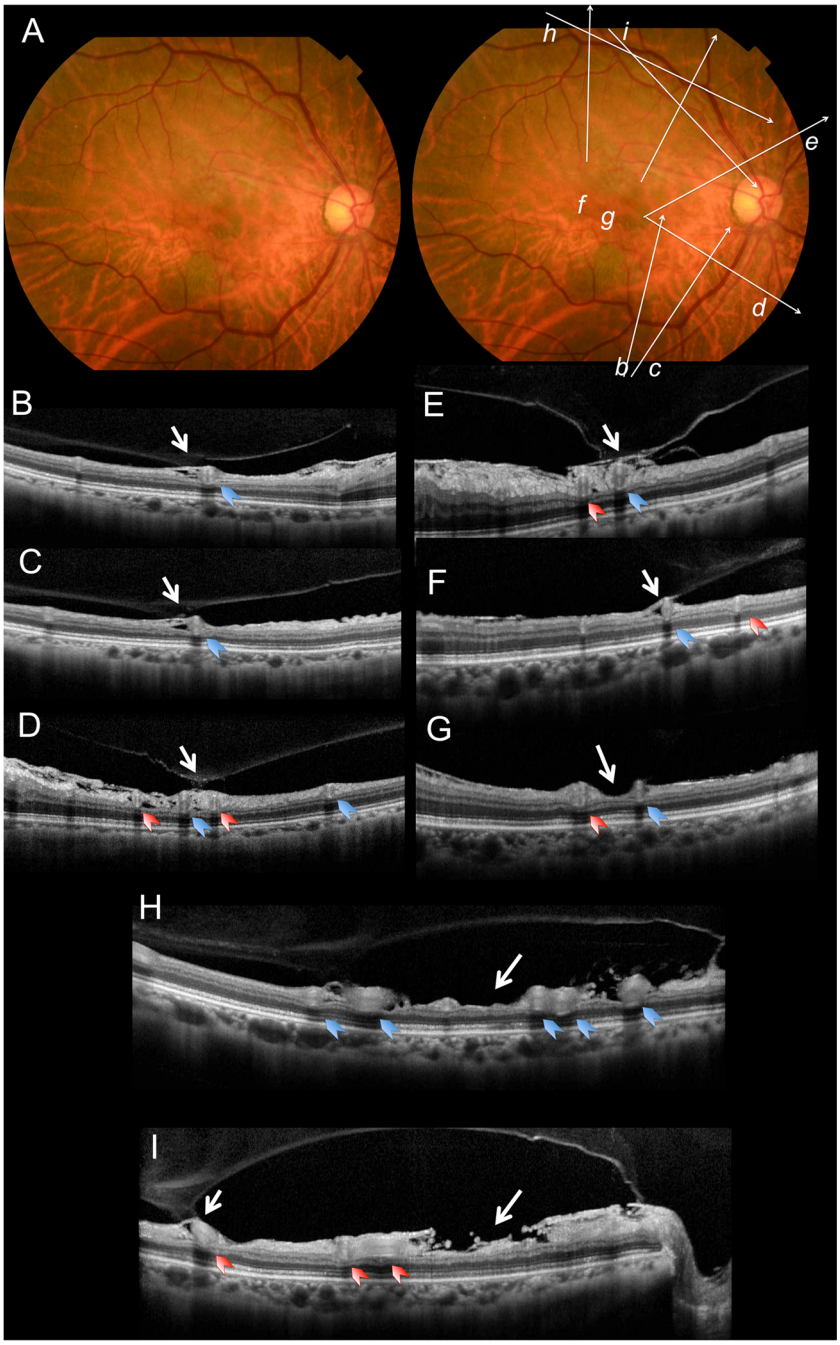


**Fig. 4** Vitreous traction on the inner retina in an eye with paravascular inner retinal defects (PIRDs) associated with an epiretinal membrane (ERM). **a** Fundus imaging shows a PIRD only along the superotemporal artery (VA, 0.5 on the Landolt chart; axial length, 22.53 mm). Optical coherence tomography (OCT) sections were taken along the *white arrows* (*b–i*). **b–d** Cross-sectional OCT images show a grade 1 PIRD of (*white arrow*) along the inferotemporal vein. Vitreoretinal adhesion is seen along the retinal vein, accompanied by the PIRD. **e–i** Cross-sectional (*e–g*) and longitudinal (*h, i*) OCT images show a grade 3 PIRD along the superotemporal vessels. **i** Vitreoretinal adhesion is seen peripapillary and peripherally. The inner surface of the PIRD remains in the area of the vitreoretinal adhesion (*white arrow*). Broad defects of the inner retinal tissue and remnants of the inner retina are seen in the areas without the vitreoretinal adhesion (*long white arrow*). *Red arrowhead* = retinal artery, *blue arrowhead* = retinal vein

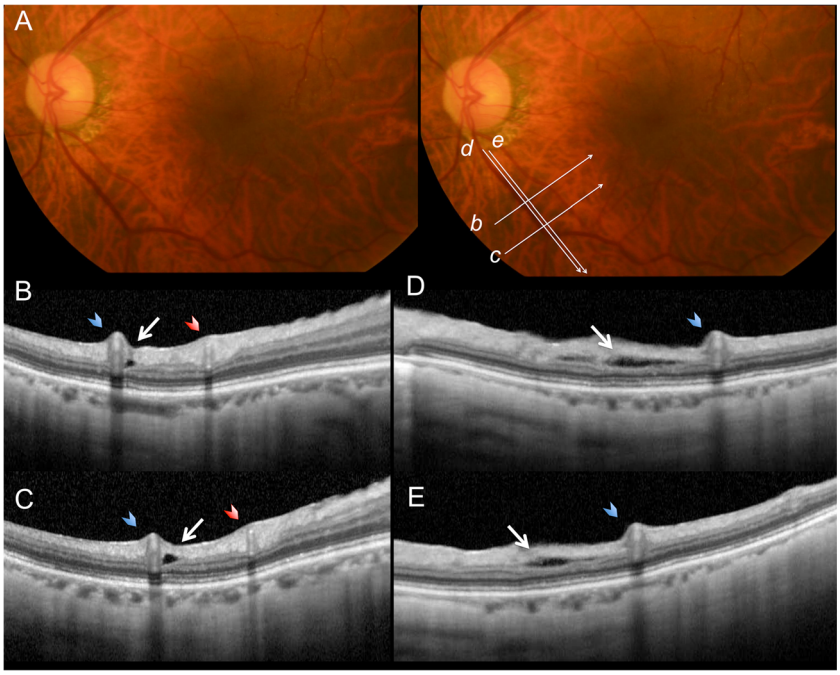


**Fig. 5** A grade 1 paravascular inner retinal defect (PIRD) associated with an epiretinal membrane (ERM). **a** The PIRD along the inferotemporal vein is not detected in images of the fundus (VA, 0.6 on the Landolt chart; axial length, 23.36 mm). Optical coherence tomography (OCT) sections were taken along the *white arrows* (*b*–*e*). **b**, **c** Cross-sectional OCT images show a cystoid space within the inner retina adjacent to the inferotemporal vein. The ERM does not appear to cause traction on the paravascular tissue. **d**, **e** Longitudinal OCT sections show a long horizontal cleavage of the inner retina along the retinal vein. *White arrow* = PIRD, *red arrowhead* = retinal artery, *blue arrowhead* = retinal vein

adhesion was seen in the paravascular areas adjacent to grade 2 or grade 3 PIRDs, and remnants of the inner retina were sometimes seen above grade 3 PIRDs.

In the current study, six eyes had PIRDs that were classified as grade 1 (19.4 %, Fig. 5), four eyes had PIRDs that were grade 2 (12.9 %, Fig. 6), and 21 eyes had PIRDs of grade 3

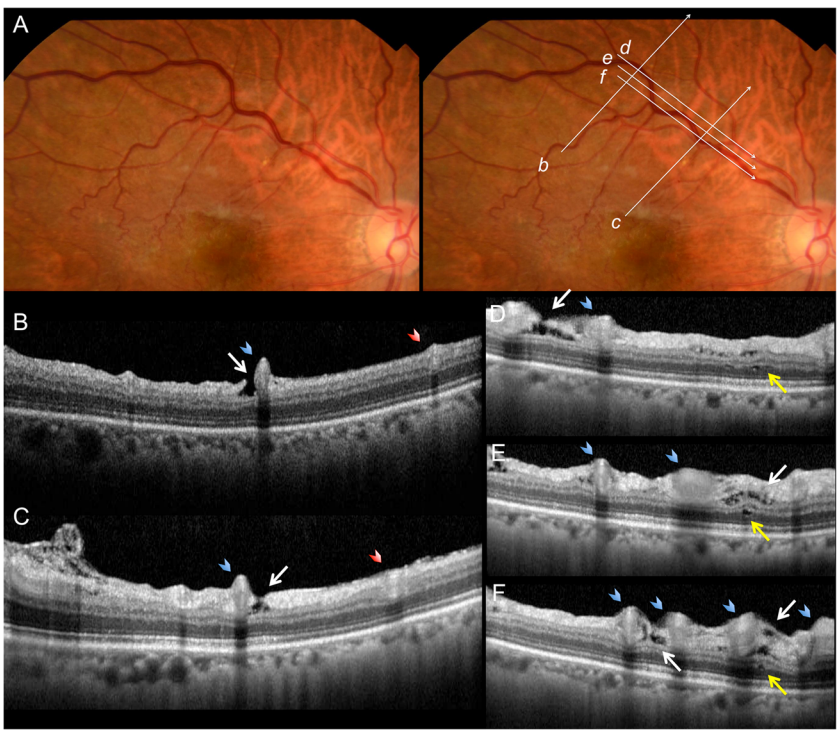


**Fig. 6** A grade 2 paravascular inner retinal defect (PIRD) associated with an epiretinal membrane (ERM). **a** A PIRD along the superotemporal vein is not detected in images of the fundus (VA, 0.8 on the Landolt chart; axial length, 22.94 mm). Optical coherence tomography (OCT) sections were taken along the *white arrows* (*b*–*f*). **b**, **c** Cross-sectional OCT images show the cleavage of the inner retina adjacent to the superotemporal vein, with no apparent defect of the inner retinal tissue. The ERM is not obvious around the PIRD or retinal vein. **d**–**f** Longitudinal OCT sections show a long horizontal cleavage of the inner retina along the vein. No apparent defect of the inner retinal tissue is seen. Cleavage is also seen in the outer plexiform layer (*yellow arrow*). *White arrow* = PIRD, *red arrowhead* = retinal artery, *blue arrowhead* = retinal vein

(67.7 %, Figs. 3 and 4). Table 2 presents the ocular characteristics in eyes with PIRDs of each grade. Eyes with PIRDs of grade 3 had a somewhat lower VA and had greater central foveal thickness, but the difference was not statistically significant. Visual field abnormalities corresponding to the locations of the PIRDs were detected in 16.7 % of eyes with grade 1 PIRDs, 33.3 % of eyes with grade 2 PIRDs, and 44.4 % of eyes with grade 3 PIRDs (Fig. 7).

## Discussion

In all of our patients, the ERMs were present in the macular area and often caused visual disturbance. Although ERMs sometimes adhered directly to the edge of a PIRD or to the major retinal vessels, most PIRDs were located outside the area that adhered to the ERM. ERMs seemed to exert traction toward to the fovea on the inner retina, resulting in the formation of inner retinal cleavages or cystoid spaces. As shown in Fig. 3, PIRDs were detected not only on the foveal side of the temporal arcade vessels, but often also on the peripheral side. It is well-known that retinal vessels can be moved by the contraction of the ERM. Vessel movement by the ERM would explain this configuration of PIRDs [14, 15]. In addition, retinal veins are more flexible and more easily moved than retinal arteries [11, 12], which would explain the higher paravenous prevalence of PIRDs. However, it remains unclear why PIRDs are observed more frequently in the superior hemisphere.

A PIRD was originally defined as a defect of the inner retina, adjacent to the major retinal vessels, that was disconnected from the optic disc [1]. In the current study, we expanded the definition of PIRDs to include inner retinal cleavages or cystoid spaces within the inner retina along the major retinal vessels. Based on OCT examinations, we classified PIRDs into three grades. Defects of the inner retinal tissue adjacent to the major retinal vessels were defined as grade 3. Paravascular inner retinal cleavages with openings to the vitreous cavity and with no apparent defect of the inner retinal tissue were defined as grade 2. Paravascular inner retinal cleavages or cystoid spaces that showed no connection to the vitreous cavity were defined as grade 1.

Hwang et al. [6] previously reported six cases of inner retinal cleavage in eyes with ERMs, and we speculate that these PIRDs could be classified as grade 2 based on the authors' description. None of the patients showed visual field defects. In our patients with grade 3 PIRDs, visual field abnormalities corresponding to the location of the PIRDs were seen more frequently (44.4 %). Muraoka et al. [1] found corresponding visual field abnormalities in 12 of 15 eyes with grade 3 PIRDs associated with ERMs without high myopia. The current grading system may reflect not only morphological changes but also functional abnormalities. In addition to the severity of PIRDs, this grading system might suggest the process of PIRD development in eyes with ERMs. However, because one of the most significant limitations of the current study is its cross-sectional design, the process of PIRD formation remains unclear. Most of our patients with PIRDs had visual disturbance due to the ERM, and it was not ethically acceptable to conduct a longitudinal observation without offering surgical treatment [16].

The current study suggests that vitreous traction contributes to the process of PIRD formation [9]. Of six eyes with grade 1 PIRDs, three (50.0 %) showed vitreous adhesion to the retinal vessels accompanied by PIRDs. The inner surface of the PIRDs sometimes appeared to be close to being torn off by the vitreous traction. In contrast, no vitreous adhesion to

**Table 2** Ocular findings in each grade of paravascular inner retinal defects associated with epiretinal membranes

| | Grade 1 | Grade 2 | Grade 3 |
|---|---|---|---|
| Number of eyes (%) | 6 (19.4 %) | 4 (12.9 %) | 21 (67.7 %) |
| Age, years | 65.7 ± 7.6 | 73.3 ± 13.6 | 71.0 ± 7.8 |
| Gender, women/men | 5/1 | 1/3 | 10/11 |
| Visual acuity, logMAR | 0.22 ± 0.19 | 0.17 ± 0.17 | 0.31 ± 0.26 |
| Axial length, mm | 23.26 ± 0.72 | 23.73 ± 0.52 | 23.50 ± 0.97 |
| Central retinal thickness, μm | 434.5 ± 166.6 | 405.8 ± 58.0 | 482.1 ± 73.6 |
| Posterior vitreous detachment, *n* (%) | 2 (33.3 %) | 4 (100.0 %) | 16 (76.2 %) |
| Pseudophakia, *n* (%) | 0 (0 %) | 1 (25.0 %) | 2 (9.5 %) |
| Location of PIRDs | | | |
| Superior hemisphere, *n* (%) | 2 (33.3 %) | 3 (75.0 %) | 10 (47.6 %) |
| Inferior hemisphere, *n* (%) | 3 (50.0 %) | 1 (25.0 %) | 1 (4.8 %) |
| Both hemispheres, *n* (%) | 1 (16.7 %) | 0 (0 %) | 10 (47.6 %) |
| Visual field defect, present/total (%) | 1/6 (16.7 %) | 1/3 (33.3 %) | 8/18 (44.4 %) |

Goldmann perimetry was not performed in one eye categorized as grade 2 and three eyes as grade 3

*PIRD* paravascular inner retinal defect, *logMAR* logarithm of the minimum angle of resolution

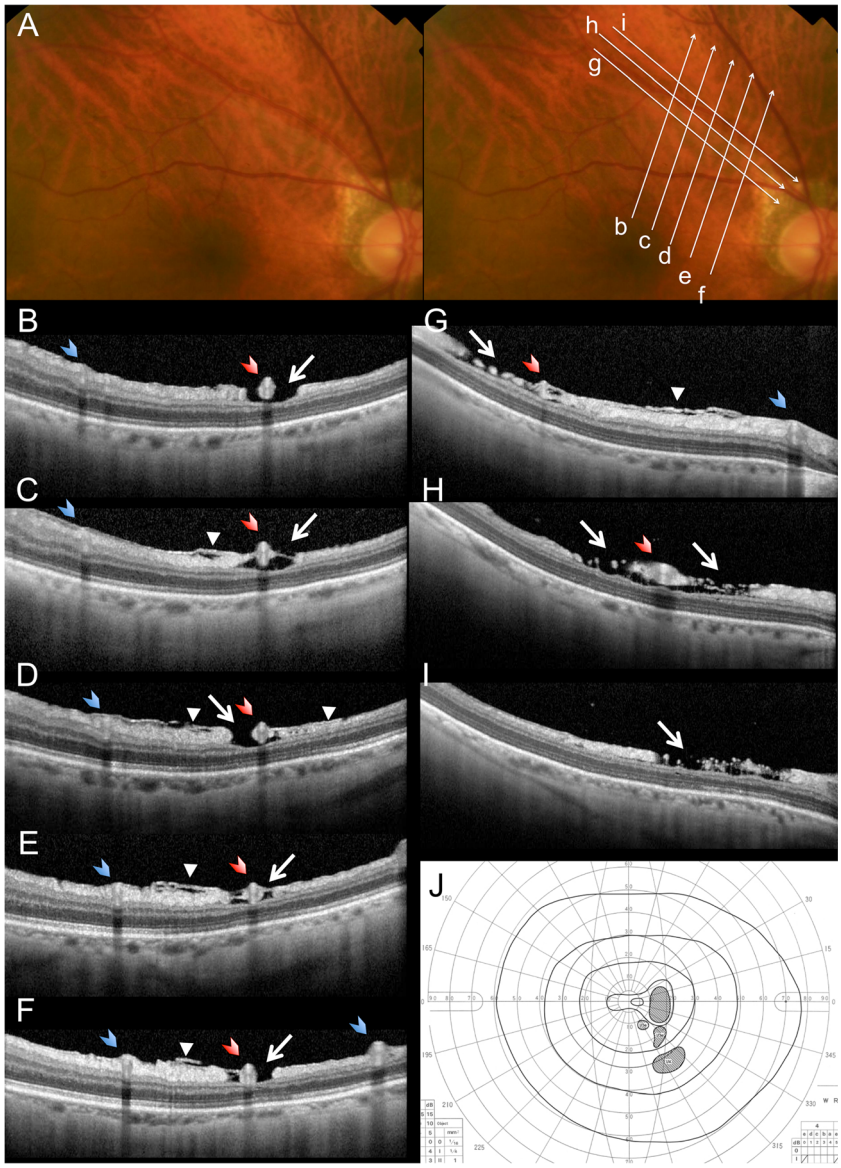


**Fig. 7** A grade 3 paravascular inner retinal defect (PIRD) associated with an epiretinal membrane (ERM). **a** Fundus imaging shows a PIRD along the superotemporal artery (VA, 0.6 on the Landolt chart; axial length, 25.00 mm). Optical coherence tomography (OCT) sections were taken along *white arrows* (*b–i*). **b–f** Cross-sectional OCT images (*b–f*) show a defect of the inner retina along the superotemporal artery. **g–i** In the longitudinal sections (*g–i*), the PIRD is deviating into the vitreous cavity, resulting in a broad defect of the inner retinal tissue. The ERM is attached to the inner edge of the PIRD and appears to induce a direct traction force on the inner retina toward the fovea. **j** A visual field abnormality is seen corresponding to the location of the PIRDs. *White arrow* = PIRD, *red arrowhead* = retinal artery, *blue arrowhead* = retinal vein

paravascular areas adjacent to grade 2 or 3 PIRDs was observed, and remnants of the inner retina were sometimes seen above the grade 3 PIRDs. Figure 7 shows the inner surface of a PIRD in the areas of a vitreoretinal adhesion, as well as the broad inner retinal defects and remnants of the inner retina in areas without vitreoretinal adhesion. In a previous study on highly myopic eyes, Shimada et al. [9] reported that paravascular lamellar holes were formed as a result of avulsion of the inner wall of a paravascular retinal cyst by vitreous traction. In a recent report, most grade 3 PIRDs (91.4 %) showed no adhesion of the posterior vitreous membrane to the inner retinal surface [1]. After a grade 1 PIRD develops as a result of the traction of the ERM, vitreoretinal traction may cause the defect on the inner surface of the PIRDs, leading to progression to grade 3.

It is generally thought that remnants of the vitreous cortex membrane in the macular area after the development of PVD play a key role in the pathogenesis of idiopathic ERM [17, 18]. However, the precise mechanism of the formation of an ERM is not fully understood [19]. A previous report described a case in which a PIRD had formed along the temporal arcade vessel that increasingly deviated toward the fovea due to the increased traction of the ERM [1]. Most of the PIRDs in our patients were consistent with this observation. However, in the current study, several PIRDs appeared to be located in paravascular areas unrelated to the traction vector induced by the ERM. At the temporal arcade vessels, which are the most frequent site of PIRDs, the posterior vitreous membrane was strongly adhered, and remnants of the inner retina were sometimes seen above grade 3 PIRDs. Migrated intraretinal glial cells, such as astrocytes or microglia, can proliferate on the retinal surface [20–23]. In some cases, it is possible that after the development of PIRDs, remnants of the inner retina may be involved in the development of an ERM.

As described above, one of the most significant limitations of the current study is its cross-sectional design. We could not fully elucidate the process of the progression of PIRDs. However, we described the prevalence, characteristics, and possible pathogenesis of PIRDs associated with ERMs. Further prospective cohort studies with longer follow-up periods are necessary to confirm the longitudinal changes and the association between PIRDs and ERMs.

**Compliance with ethical standards**

**Funding** No funding was received for this research.

**Conflict of interest** All authors certify that they have no affiliations with or involvement in any organization or entity with any financial interest or non-financial interest in the subject matter or materials discussed in this manuscript.

**Ethical approval** This prospective study was approved by the ethics committee of Kagawa University Faculty of Medicine and were conducted in accordance with the tenets of the 1964 Declaration of Helsinki.

**Informed consent** Written informed consent was obtained from each subject before any study procedures or examinations were performed.

## References

1. Muraoka Y, Tsujikawa A, Hata M, Yamashiro K, Ellabban AA, Takahashi A, Nakanishi H, Ooto S, Tanabe T, Yoshimura N (2015) Paravascular inner retinal defect associated with high myopia or epiretinal membrane. JAMA Ophthalmol 133:413–420
2. Chihara E (2015) Myopic cleavage of retinal nerve fiber layer assessed by split-spectrum amplitude-decorrelation angiography optical coherence tomography. JAMA Ophthalmol 133:e152143
3. Chihara E, Chihara K (1992) Apparent cleavage of the retinal nerve fiber layer in asymptomatic eyes with high myopia. Graefes Arch Clin Exp Ophthalmol 230:416–420
4. Komeima K, Ito Y, Nakamura M, Terasaki H (2010) Inner retinal cleavage associated with idiopathic epiretinal membrane. Retin Cases Brief Rep 4:132–134
5. Komeima K, Kikuchi M, Ito Y, Terasaki H, Miyake Y (2005) Paravascular inner retinal cleavage in a highly myopic eye. Arch Ophthalmol 123:1449–1450
6. Hwang YH, Kim YY, Kim HK, Sohn YH (2015) Characteristics of eyes with inner retinal cleavage. Graefes Arch Clin Exp Ophthalmol 253:215–220
7. Tuulonen A, Yalvac IS (2000) Pseudodefects of the retinal nerve fiber layer examined using optical coherence tomography. Arch Ophthalmol 118:575–576
8. Ohno-Matsui K, Hayashi K, Tokoro T, Mochizuki M (2006) Detection of paravascular retinal cysts before using OCT in a highly myopic patient. Graefes Arch Clin Exp Ophthalmol 244:642–644
9. Shimada N, Ohno-Matsui K, Nishimuta A, Moriyama M, Yoshida T, Tokoro T, Mochizuki M (2008) Detection of paravascular lamellar holes and other paravascular abnormalities by optical coherence tomography in eyes with high myopia. Ophthalmology 115:708–717
10. Uji A, Yoshimura N (2015) Application of extended field imaging to optical coherence tomography. Ophthalmology 122:1272–1274
11. Muraoka Y, Tsujikawa A, Murakami T, Ogino K, Kumagai K, Miyamoto K, Uji A, Yoshimura N (2013) Morphologic and functional changes in retinal vessels associated with branch retinal vein occlusion. Ophthalmology 120:91–99
12. Muraoka Y, Tsujikawa A, Kumagai K, Akagi-Kurashige Y, Ogino K, Murakami T, Miyamoto K, Yoshimura N (2014) Retinal vessel tortuosity associated with central retinal vein occlusion: an optical coherence tomography study. Invest Ophthalmol Vis Sci 55:134–141
13. Kumagai K, Tsujikawa A, Muraoka Y, Akagi-Kurashige Y, Murakami T, Miyamoto K, Yamada R, Yoshimura N (2014) Three-dimensional optical coherence tomography evaluation of vascular changes at arteriovenous crossings. Invest Ophthalmol Vis Sci 55:1867–1875
14. Nitta E, Shiraga F, Shiragami C, Fukuda K, Yamashita A, Fujiwara A (2013) Displacement of the retina and its recovery after vitrectomy in idiopathic epiretinal membrane. Am J Ophthalmol 155:1014–1020, e1011
15. Kofod M, la Cour M (2012) Quantification of retinal tangential movement in epiretinal membranes. Ophthalmology 119:1886–1891
16. Jackson TL, Nicod E, Angelis A, Grimaccia F, Prevost AT, Simpson AR, Kanavos P (2013) Pars plana vitrectomy for vitreomacular traction syndrome: a systematic review and metaanalysis of safety and efficacy. Retina 33:2012–2017
17. Kishi S, Demaria C, Shimizu K (1986) Vitreous cortex remnants at the fovea after spontaneous vitreous detachment. Int Ophthalmol 9:253–260
18. Kishi S, Shimizu K (1994) Oval defect in detached posterior hyaloid membrane in idiopathic preretinal macular fibrosis. Am J Ophthalmol 118:451–456
19. Bu SC, Kuijer R, Li XR, Hooymans JM, Los LI (2014) Idiopathic epiretinal membrane. Retina 34:2317–2335
20. Bellhorn MB, Friedman AH, Wise GN, Henkind P (1975) Ultrastructure and clinicopathologic correlation of idiopathic preretinal macular fibrosis. Am J Ophthalmol 79:366–373
21. Clarkson JG, Green WR, Massof D (1977) A histopathologic review of 168 cases of preretinal membrane. Am J Ophthalmol 84:1–17
22. Green WR, Kenyon KR, Michels RG, Gilbert HD, De La Cruz Z (1979) Ultrastructure of epiretinal membranes causing macular pucker after retinal re-attachment surgery. Trans Ophthalmol Soc U K 99:65–77
23. Hui YN, Goodnight R, Zhang XJ, Sorgente N, Ryan SJ (1988) Glial epiretinal membranes and contraction. Immunohistochemical and morphological studies. Arch Ophthalmol 106:1280–1285